26th ABCM International Congress of Mechanical Engineering
November 22-26, 2021. Florianópolis, SC, Brazil

COBEM-2021-0584
CASE STUDIES OF MODELLING, STRUCTURAL AND VIBRATION ANALYSIS OF CENTRIFUGAL COMPRESSOR IMPELLERS

Lucas Nunes de Carvalho
Diego Zilli Lima
Daniel Jonas Dezan
Federal University of ABC – UFABC
Av. dos Estados, 5001 - Bangú, 09210-580, Santo André/SP, Brazil
l.carvalho@ufabc.edu.br
diego.zilli@aluno.ufabc.edu.br
daniel.dezan@ufabc.edu.br

Elóy Esteves Gasparin
Vitor Cesar Nogueira Mattos
Leandro Oliveira Salviano
UNESP – Ilha Solteira
Av. Brasil Sul, 56 – Centro, 15385-000, Ilha Solteira/SP, Brazil
eloy.gasparin@unesp.br
vitor.mattos@unesp.br
leandro.salviano@unesp.br

Paulo Eduardo Batista de Mello
Centro Universitário FEI
Av. Humberto de Alencar Castelo Branco, 3972-B - Assunção, São Bernardo do Campo – SP
pmello@fei.edu.br

Fabio Saltara
Jurandir Itizo Ynagihara
USP - University of São Paulo
Av. Prof. Mello Moraes, 2231 - Cidade Universitária, 05508-080, São Paulo/SP, Brazil
fsaltara@usp.br
jiy@usp.br

Wallace Gusmão Ferreira
Federal University of ABC – UFABC
Av. dos Estados, 5001 - Bangú, 09210-580, Santo André/SP, Brazil
wallace.ferreira@ufabc.edu.br

Abstract. *The oil extraction on off-shore platforms needs to deal with the CO2 present in the wells with a high oil-gas ratio. In addition to the oil industry, there is also a global environmental motivation to deal with a large amount of CO2 present in Earth's atmosphere. The most recent researches in the area propose the use of centrifugal compressors to compress the gas and treat it, or even insert it back in the underground wells. This study presents an evolution of modeling and analysis of centrifugal compressors through three case studies. In the first case, using a model known as Eckardt Compressor, and analyzing only the impeller blades, the structural safety factors are calculated, and the possible resonance points are verified using the Campbell diagram. In the second case, using a compressor of stage 1 treatment of supercritical CO2, the ideal material for the impeller is determined, an early design of the impeller disc is performed and, through a previous Design of Experiments analysis, a new geometry that meets the structural safety factors including the burst speed is proposed. In the third case, a stage 4 compressor model used in sCO2 treatment is used, and due to the high-pressure ratio, the need to consider the impeller backplate pressure is evaluated, then an analytical model is identified for the application of the so-called "backpressure", and to avoid changing the geometry of the blades, a parametric optimization of the disc geometry is performed with DOE, to meet the structural safety factors.*

Keywords: *centrifugal compressors, Campbell diagram, structural analysis, optimization, design of experiments.*

1. INTRODUCTION

The energy sector in industry rises day by day, and the available technology for application must rise with it. The necessity for clean and renewable energy sources increases together with a global environmental motivation to deal with a large amount of CO_2 present in Earth's atmosphere, but oil still is the most used energy source in the world (IEA, 2019).

Oil extraction on off-shore platforms needs to deal with the CO_2 present in the wells with a high oil-gas ratio. The most recent researches in the area propose the use of centrifugal compressors to compress the gas and treat it, or even insert it back in the underground wells, for example, supercritical CO_2 can be used as a working fluid for power generation systems (White et al., 2020). Gas turbomachinery components must be designed against specific failure modes, in this study the modes considered are *static*, *burst*, and *dynamic* (which can induce phenomena as flutter, stall, and/or surge) (Braembussche, 2019; Saravanamuttoo et al., 2017).

The current work is part of a project underway in RCGI (Research Centre for Gas Innovation): *Simulation and Optimization of CO2 and CH4 Compressors at Supercritical Conditions.* It presents the evolution of the process of modeling and analysis of centrifugal compressors being developed in the current project through three practical case studies.

The focus is on the structural and dynamics requirements of the impellers, so the analysis of the fluid conditions and CFD (computational fluid dynamics) simulations will not be detailed here. The first case is a validation of the analysis method based on well-known published results. The second and third cases are compressor impeller geometries currently being designed in the context of the project to attend to the compression demands of CO_2 at supercritical conditions.

In each case study, a brief description of the simulation methodology applied will be described and the respective results will be presented and discussed.

2. CASE STUDIES

2.1 Case 1

The first case used Eckardt's impeller based on (Cho et al., 2012; Oh et al., 1997) to validate the analysis process. One-way fluid-structure interaction (FSI) analysis was performed, with the CFD mesh mapped to finite element mesh and the aerodynamic loads used as boundary conditions in static structural analysis (Yin et al., 2017). In addition to the pressure field, inertial load due to rotational speed was also employed.

The CFD analysis was performed considering the cyclic symmetry of the impeller. The boundary conditions used were total pressure and total temperature at the inlet equals 1,0133 bar and 288,1 K, respectively, and mass flow at the outlet equal to 5,31 kg/s, using air as an ideal gas. The turbulence model used was the k-ε and the compressor rotational speed was equal to 14000 rpm.

For the structural analysis, the material considered was AL7075, with Young's modulus 71 GPa and Poisson's ratio 0,33. The first analysis performed only considered the blade, this simplification considers the fact that the impeller disc has a much greater stiffness than the blade. The boundary condition for the displacements in this type of analysis is to fix the blade hub face, physically this means a disk with infinite stiffness. The loads adopted in the analysis were both the pressure mapped from the CFD analysis as well as the rotational speed of 14000 rpm.

The analysis of the impeller model considered that the connection between the disc and the shaft is fixed, as can be seen in Figure 1. The loads employed were the same as for the single-blade model, but with the addition of pressure mapped on the hub. As the calculated pressures in the CFD analysis are for only one sector, to expand the field it is necessary to perform the transformation around the axis of rotation to apply the pressure load on all blades and all surfaces of the hub.

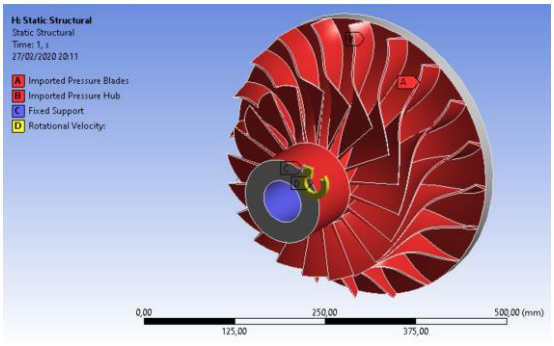

Figure 1: Impeller structural model.

The last part of the analysis carried out was the modal analysis to obtain possible points of resonance. For this analysis, the procedure used was the elaboration of the Campbell diagram. To create the diagram, only one impeller sector was used, and the cyclic symmetry condition was applied in the structural model. The tool used was the ANSYS Mechanical and the stress stiffening effects were considered through pre-stressed modal analysis. As the cyclic symmetry model available in the computational tool does not allow the use of non-symmetric matrices, gyroscopic effects were neglected.

2.1.1 Results

The first results obtained were related to fluid dynamic analysis. In Table 1, the relative error did not exceed the value of 5% from the experimental data.

Table 1: CFD analysis results, Case 1.

Parameter	CFD analysis	Experimental	Relative error
Isentropic efficiency	0,927	0,889	4,30 %
Pressure ratio	1,87	1,91	1,89 %

With the CFD analysis completed, it was possible to obtain the pressure field around the blade and hub to be mapped to the structural mesh. On the left side of Figure 2, it is possible to see the pressure field around the blade obtained by the CFD simulation, on the right side is represented the load completely mapped on the impeller surfaces.

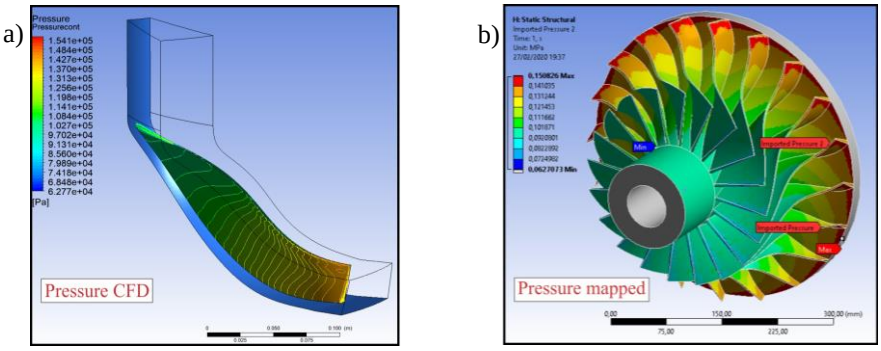

Figure 2: Pressure mapping: a) CFD pressure results; b) Pressure mapped to the structural model.

The first structural analysis considered a single sector of the impeller. Two load cases were applied, in the first, only the aerodynamic loading was applied, and in the second, both the aerodynamic and the rotational speed of 14000 rpm. In Figure 3 are the results with both pressure and rotation. Figure 3a shows the total displacements for the second load case, the maximum was 0,44 mm, located just below the leading edge. The tip displacement is directly linked to the gap between the blade and the shroud, one of the main factors of loss of efficiency in open impeller compressors.

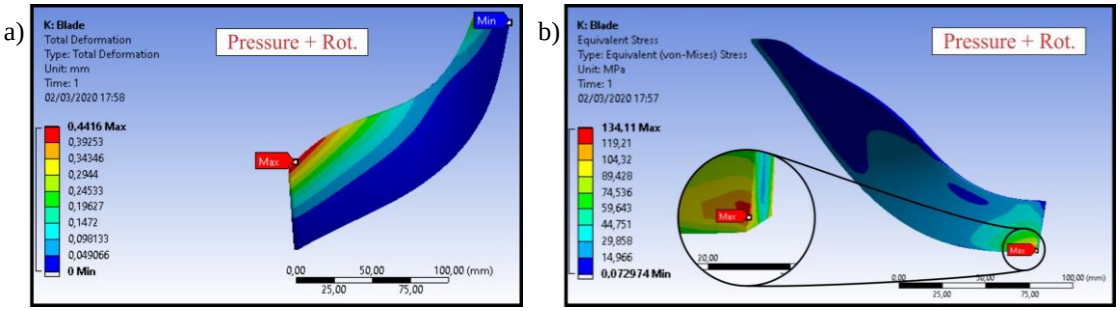

Figure 3: Eckardt single blade results: a) Total displacement; b) Equivalent stress.

In Figure 3b, the stress results are shown. The maximum stress obtained was 134 MPa, the location of the highest stress concentration was just above the hub on the trailing edge. Considering that the yield stress of AL7075 alloy is 503

MPa, the stress levels on the blade are safe. This type of analysis, although simple, allows checking quickly if blade thickness is adequate for the project.

The next results found were those of the analysis carried out considering the complete impeller. As for the single-blade model, two load cases were considered, pressure and pressure plus rotational speed. The total displacements obtained for the two conditions are shown in Figure 4. When comparing the case with aerodynamic pressure plus rotation, displacements are higher, from 0,44 mm to 0,60 mm. This is because the disc is flexible, and the resultant inertial loading is in the same direction as the pressure loading.

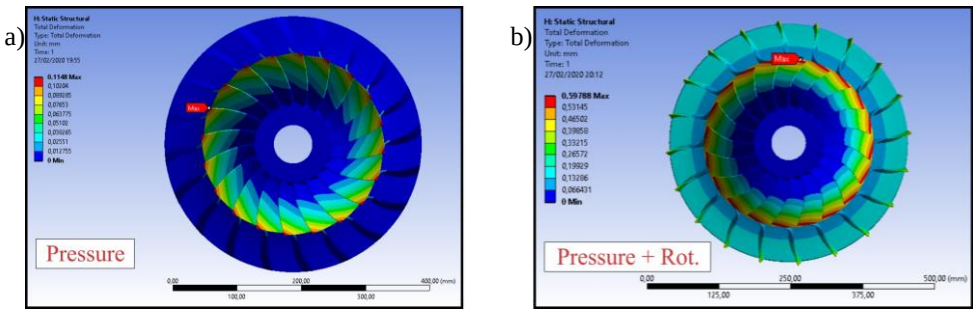

Figure 4: Eckardt total displacements: a) Rotation only; b) Pressure and rotation.

As for the stresses in the impeller, the results obtained are in Figure 5. The maximum stress value obtained was 238,6 MPa, in the region of connection with the shaft, this value is still well below the yield limit of 503 MPa, but details about the shaft and the impeller connection are missing, it must not be accounted for. Figure 5a is the stress distribution generated by pressure load only, as can be seen, the maximum stress value found was 5,68 MPa, lower when compared to the result for the model with a single blade (Figure 3b) caused by a greater load distribution due to the not infinite stiffness of the disk. An interesting result obtained was the location of the maximum stress when considering the complete impeller, this point was on the leading edge close to the hub. Although this is a static analysis, and the applied pressure does not vary over time, pressure fluctuations will occur during compressor operation, even so, this type of analysis is fundamental to identify stress concentrators that may cause the nucleation of cracks and, consequently, the reduction of the life of the compressor. Comparing the compressor studied by Chen et al., (2017), Figure 5b, which had a failure that originated in the leading edge close to the hub, it can be observed that the results obtained with the finite element model are following what was observed in the real operation.

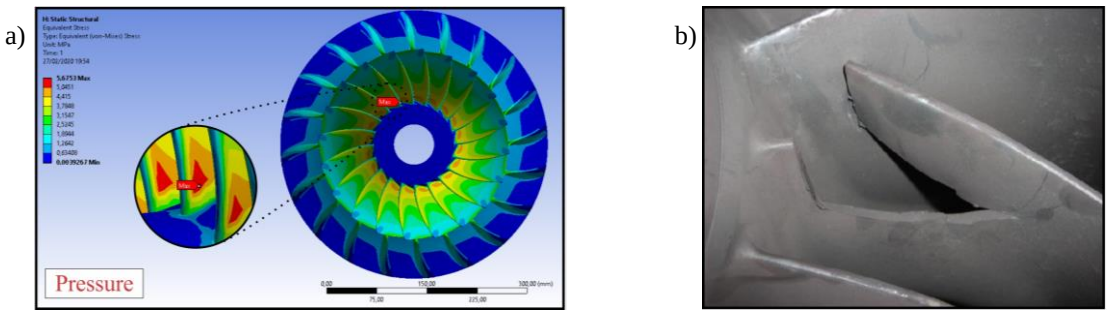

Figure 5: Eckardt stress results: a) Simulation (present study); b) Blade crack reported by Chen et al., (2017).

Figure 6 is the Campbell Diagram for disk modes with 2, 3, and 4 nodal diameters. According to Kushner et al., (2000); Wang et al., (1999), the most worrying modes are those with smaller nodal diameters, due to their greater capacity to transfer energy to the structure. In Figure 6, it is possible to see crossing points between the modes and lines of 18x, 17x, 15x, 14x, and 12x harmonic excitations. These crossings can indicate resonances and more detailed analysis should be considered. For this study, the analysis followed up to this point, because there is not enough geometric data from Eckardt impeller A to verify if these critical points found can cause resonance. Resonance verification methods considering frequency cancellation can be found in the references (Kushner et al., 2000; Singh et al., 2003; Wang et al., 1999), the method known as “Singh's Advanced Frequency Evaluation” (SAFE), first presented in (Singh et al., 1988), together with the Campbell Diagram method, are the most used methods in the industry.

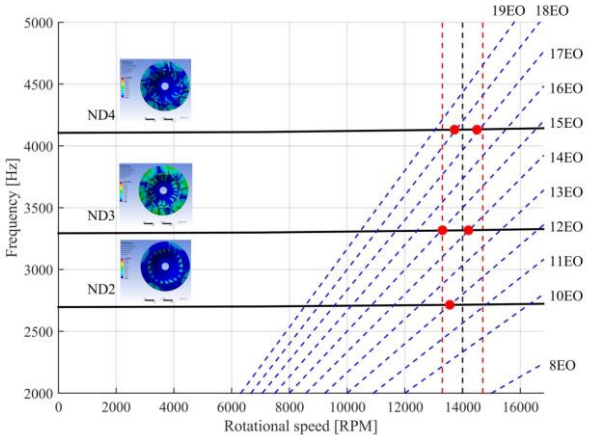

Figure 6: Campbell Diagram: horizontal lines represent the natural frequencies of each nodal diameter, red dashed vertical lines represent the safe margin of 5% in relation to operational speed, diagonal lines are engine order and red dots the crossing points.

2.2 Case 2

The impeller studied, in this case, is from the first stage of a centrifugal compressor working with supercritical CO_2 (sCO_2). The compressor operates at 12500 rpm, with an inlet pressure of 400 kPa, temperature of 320 K, and 55,56 kg/s mass flow of real gas Carbon Dioxide. The blades' geometry was generated using ANSYS Vista CCD, and a Turbomachinery CFD analysis was taken in CFX to obtain the pressure field of the fluid and map it to the impeller geometry, which was then analyzed in a Static Structural analysis, using ANSYS Mechanical (Figure 7a and b).

Following the method proposed by Dowson et. al. (2008), the chosen material was the 13Cr-4Ni (UNS S42400), a Stainless Steel, with a yield strength of 552 MPa (σ_y), ultimate strength of 689 MPa (σ_u), and Young's modulus 220 GPa. The considered design requirements are (Armand, 1995):

- Safety factor based on yield strength: $SF_{yd} = 1{,}1$ $\left(max.stress \leq \frac{\sigma_y}{1{,}1}\right)$;
- Safety factor based on ultimate strength: $SF_{ud} = 1{,}5$ $\left(max.stress \leq \frac{\sigma_u}{1{,}5}\right)$;
- Safety factor on the maximum stress at 120% speed (burst condition): $SF_{ub} = 1{,}1$ $\left(max.stress \leq \frac{\sigma_u}{1{,}1}\right)$.

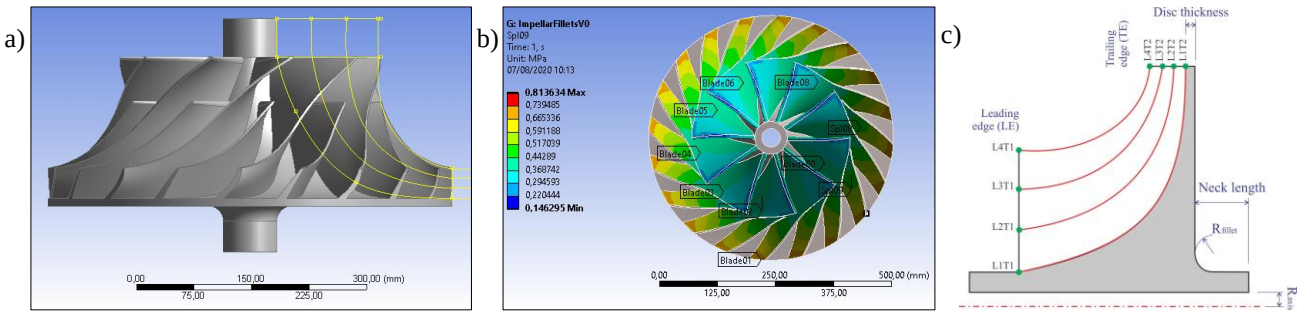

Figure 7: a) Case 2 baseline geometry; b) mapped pressure from CFD analysis; c) geometry parameters.

This model was parameterized using ANSYS. This way, any modifications needed could be easily done, and the model is prepared for a possible Design of Experiments (DOE) optimization. Twelve parameters were defined, eight of them are related to the thickness of the blades, four on the leading edge and four on the trailing edge, equally distributed from hub to shroud (Figure 7c and Table 2). The other parameters defining the blade geometry were ignored because changing them would cause much more difference in the fluid results, and as the aim is to analyze only the structural requirements, more complexity would make this study inviable.

Table 2: Thickness distribution and impeller parameters for the baseline geometry and proposed modification, Case 2.

Parameter	Baseline [mm]	Proposed Model [mm]	Parameter	Baseline [mm]	Proposed Model [mm]
L1T1	7,5	8,25	L4T1	3,00	3,30
L1T2	10,00	11,00	L4T2	3,00	2,75
L2T1	6,00	6,60	Rfillet	20,00	20,00
L2T2	7,61	8,43	Raxis	15,00	15,00
L3T1	4,50	4,95	Neck length	60,00	60,00
L3T2	5,32	5,85	Disc thick.	10,00	10,00

2.2.1 Results

Following, the results of Case 2. For the baseline, the criteria of normal operation condition are met (Figure 8). It can be seen in Table 3, that the baseline geometry doesn't meet the criteria of the burst speed, and a new geometry is needed.

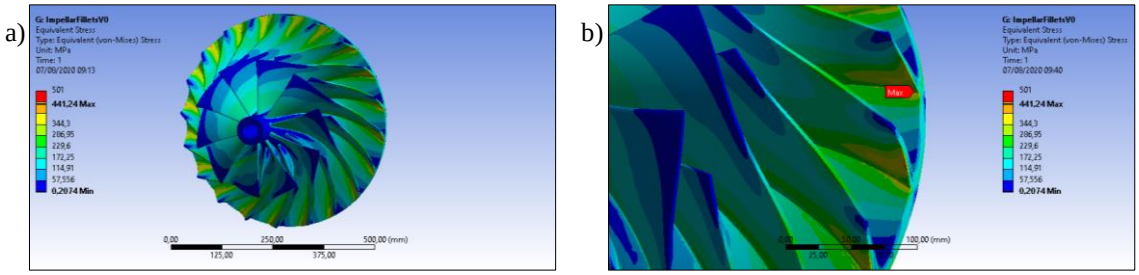

Figure 8: Stress on the baseline geometry, Case 2.

As mentioned above, Table 2 shows the parameters of the proposed model. A DOE analysis was performed to firstly obtain the more sensible parameters and then propose a new geometry, this approach was used to easily obtain a model that met the structural requirements. For the proposed model, Figure 9 shows that the maximum stress in both cases remains at the hub, and near the trailing edge of the blades.

Table 3: Results for the Case 2

Model	Speed [RPM]	Max. Stress [MPa]	SFyd (>1,1)	SFud (>1,5)	SFub (>1,1)	Pass
Baseline	12500	441	1,25	1,56	-	No
	15000	638	-	-	1,09	
Proposed Model	12500	407	1,36	1,69	-	Yes
	15000	588	-	-	1,18	

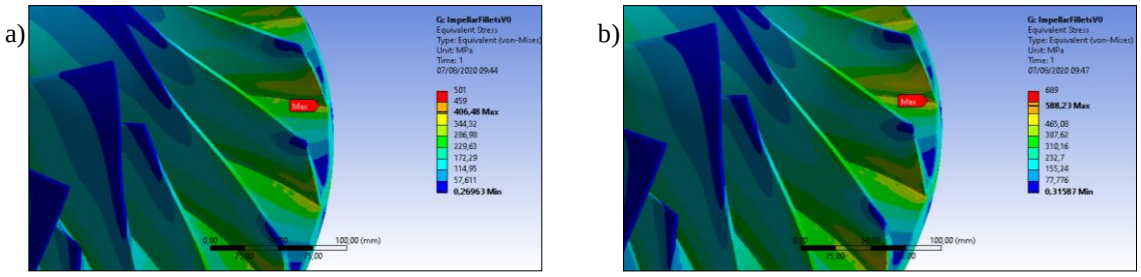

Figure 9: Stress on the proposed geometry: a) Nominal speed; b) Burst speed.

The proposed modified geometry passes the criteria of both nominal speed and burst speed. It is important to note that modifying the blade thickness distribution, the flow passage changed and a new CFD analysis would be ideal, this way, a perfect analysis would be done with a Two-Way Fluid-Structure Interaction (FSI) analysis, to track the structural feasibility of the compressor and still guarantee its compressing efficiency.

2.3 Case 3

As in case 2, the impeller used in this also works with supercritical CO_2, but this one is a fourth stage compressor, so the compressing ratio is much greater, and to attend to the compressibility needed, the aspect ratio became thinner (Figure 10), as compared to the first state, Figure 7. In this case, the study of the backpressure made essential, once the high pressures involved, combined with the aspect ratio of the blades, resulted in both much higher deformation and stresses. The same material was used, and the design requirements were maintained.

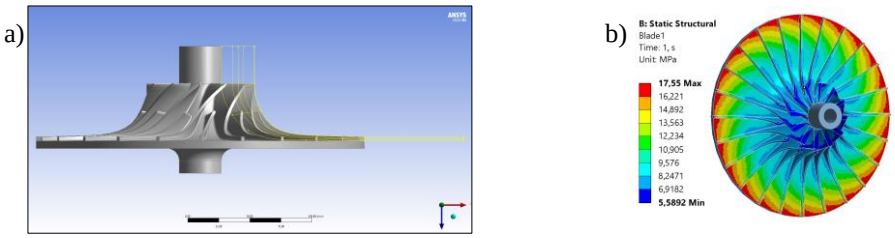

Figure 10: Case 3 a) Baseline geometry; b) Mapped pressure from CFD analysis.

The leakage of the fluid on the hub cavity creates the backpressure (Figure 11). As mentioned, this shows up here, primarily because of the distribution of the pressures in the impeller (5,59 – 17,55 MPa). In this case, without considering this relevant pressure, the deformation and stress of the model would be incorrect. Younsi et. al. (2019) applied a simplified pressure distribution that presented a good correlation with 3D CFD models and physical experiments. In the present study, it was adopted a similar approach to estimate the pressure distribution.

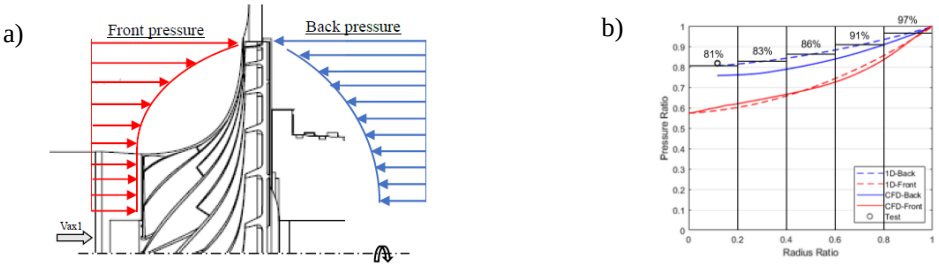

Figure 11: Pressure distribution model: a) Impeller front and back pressure approximated profile; b) Radial distribution of the pressure, adapted from Younsi & Hypolite, (2019).

To better understand the phenomena involved, two analyses were taken separately, one with a rotation only load, and one loaded with both rotation and pressure, in that, both the front pressure and the backpressure were included together.

First, it is possible to see that the deformation of the impeller goes in an “umbrella-like” format, and the displacements with the pressure included are about 8 times greater than with the rotation only load (Figure 12). This is the first indicator that – in this case – the inertia of the impeller is less impactful than the pressure applied on it.

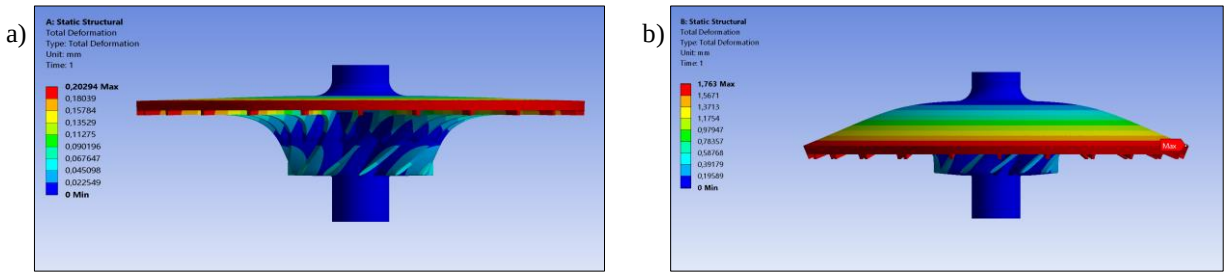

Figure 12: Baseline displacements: a) Rotation only; b) Rotation and pressure loads.

Following, there is the stress on the impeller. When the load case is the rotation only (Figure 13), the model may appear as it would meet the criteria (490 MPa), but with the pressure included (Figure 14), the result shows maximum stress of 1462 MPa, which is very above the allowable stress.

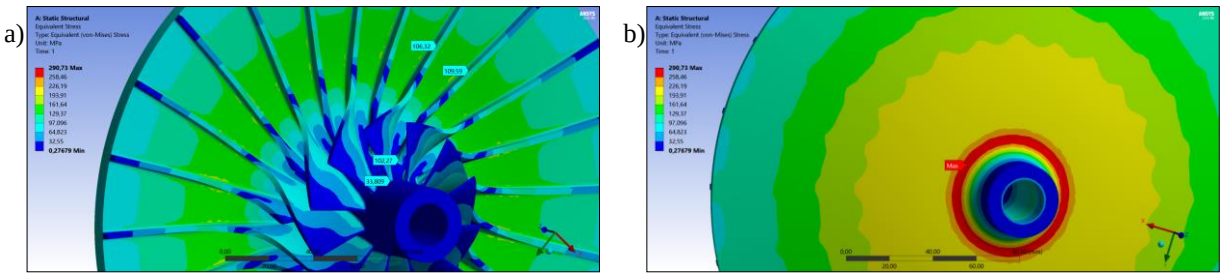

Figure 13: Baseline stress with rotation only load: a) Front b) Back.

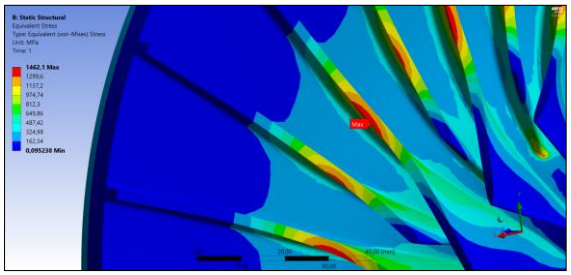

Figure 14: Baseline stress with rotation and pressure.

There is a necessity to modify the geometry to meet the criteria. The geometry of the impeller can be divided into two main areas, as such, the blades generated by the CFD analysis, and the disc geometry manually created based on the blades. So, at first, two models were proposed, Model B, which only duplicates the thickness of the blades, and Model C that instead duplicates the disc thickness (Table 4). This approach was used to understand which of these parameters is more impactful on the results. With those results, a third model was proposed (Model D), with a variable thickness on the disc and adjustments on the fillet and neck length. Both those parameters and the representation of the Model D geometry can be seen in Figure 15.

Table 4: Parameter values for the baseline geometry and proposed models.

Parameter	**Baseline [mm]**	**Model B [mm]**	**Model C [mm]**	**Model D [mm]**
Blade thick.	2,50	2,50	5,00	2,50
Blade Fillet	1,00	1,00	1,00	1,00
Disc Root thick.	6,00	12,00	6,00	17,00
Disc Top thick.	6,00	12,00	6,00	10,00
Rfillet	10,00	10,00	10,00	30,00
Raxis	10,00	10,00	10,00	10,00
Neck Length	20,00	20,00	20,00	45,00

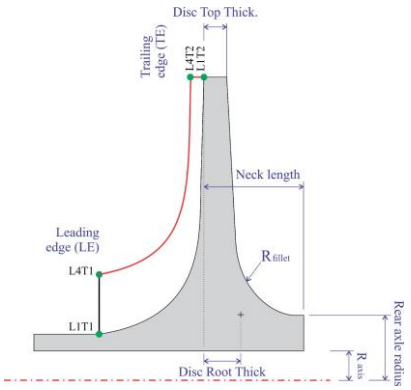

Figure 15: Impeller geometry parameters, Case 3.

2.3.1 Results

The results for Case 3 can be seen in Table 5 and Figure 16. As models B and C did not pass the criteria for the normal condition, the burst condition analysis was made only for Model D.

Table 5: Results for the case 3

Model	Speed [RPM]	Max. Stress [MPa]	Max. Disp. [mm]	SFyd (>1,1)	SFud (>1,5)	SFub (>1,1)	Pass
Baseline	19540	1462	1,763	0,38	0,47	-	No
Model B	19540	888	0,657	0,62	0,78	-	No
Model C	19540	1177	1,315	0,47	0,59	-	No
Model D	19540	406	0,284	1,36	1,70	-	Yes
Model D (burst condition)	23448	484	0,298	-	-	1,43	

Comparing the models B and C it is possible to notice that, besides the fact that increasing blades thickness showed an improvement in the results of stress and deformations, the disc thickness is the most important factor to have in mind in this case, which is good because, at first, a new CFD analysis is undesirable, and the structural criteria can be met just modifying the disc geometry. For that, a new model was proposed, with variable thickness in the disc and alteration on the fillets.

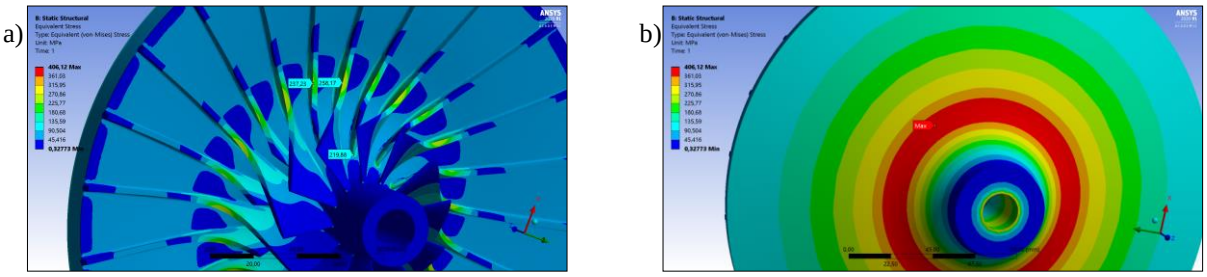

Figure 16: Model D stresses: a) Front; b) Back.

Model D has passed the criteria. It is important to note some points:

- The deformation of approximately 0,3mm can affect the leakage on the blade tip, and thus, the backpressure. So, a Two-Way FSI analysis would be ideal to identify the real pressure on the impeller.
- The criteria were met by a relatively large margin, so there is still space for optimization on the impeller geometry.

3. CONCLUSION

As stated before the current work is part of a project underway in RCGI (Research Centre for Gas Innovation): *Simulation and Optimization of CO_2 and CH4 Compressors at Supercritical Conditions.* It was presented the process of modeling and analysis of centrifugal compressors being developed in the project through three practical case studies.

The first case used Eckardt's impeller from published results of literature to validate the analysis process. The second case studied the impeller from the first stage of a centrifugal compressor working with supercritical CO_2 (sCO_2) and in case 3 the impeller is from a fourth stage CO_2 compressor.

The results covered linear static analysis with both centrifugal loads and pressure mapped from prior CFD simulations in a one-way fluid-structure interaction procedure. In addition, vibration analysis (normal modes) was performed with the generation of Campbell diagrams to verify possible resonance points in the operational region. The impeller geometries were parameterized and DOE studies permitted fine adjustment of shape parameters to achieve desired structural stress and displacement responses for the materials used.

The results found are following the previous simulation and experimental results from the literature and the structural analysis process is validated for the preliminary design of centrifugal compressor impellers. The next research steps will cover two-way fluid-structure interactions analyses to model and evaluate more complex dynamic structural phenomena and multidisciplinary optimization.

4. ACKNOWLEDGEMENTS

We gratefully acknowledge the support of the RCGI – Research Centre for Gas Innovation, hosted by the University of São Paulo (USP) and sponsored by FAPESP – São Paulo Research Foundation (2014/50279-4 and 2020/15230-5) and Shell Brasil, and the strategic importance of the support given by ANP (Brazil's National Oil, Natural Gas, and Biofuels Agency) through the R&D levy regulation.

5. REFERENCES

Armand, S. C. (1995). Structural Optimization Methodology for Rotating Disks of Aircraft Engines. *NASA Technical Memorandum*, *4693*(November), 20.

Braembussche, R. Van den. (2019). *Design and Analysis of Centrifugal Compressors* (1st ed.). Wiley - ASME Press. https://www.wiley.com/en-us/Design+and+Analysis+of+Centrifugal+Compressors-p-9781119424109

Chen, X., Xu, S., Wang, X., Ju, W., Yang, S., & Meng, J. (2017). Research on Failure of Semi-Open Centrifugal Impeller Under Aerodynamic Load. *Proceedings of the ASME Turbo Expo 2017: Turbomachinery Technical Conference and Exposition*, *Volume 7B*, 1–11. https://doi.org/10.1115/GT2017-64564

Cho, S.-Y., Ahn, K.-Y., Lee, Y.-D., & Kim, Y.-C. (2012). Optimal Design of a Centrifugal Compressor Impeller Using Evolutionary Algorithms. *Mathematical Problems in Engineering*, *2012*, 1–22. https://doi.org/10.1155/2012/752931

Dowson, P., Bauer, D., & Laney, S. (2008). Selection of Materials and Material Related Processes for Centrifugal Compressors and Steam Turbines in the Oil and Petrochemical Industry. *Proceedings of the 37th Turbomachinery Symposium*, 189–209. https://doi.org/https://doi.org/10.21423/R1SS8C

IEA. (2019). *Total primary energy supply (TPES) by source, World 1990-2017*. IEA. https://www.iea.org/data-and-statistics?country=WORLD&fuel=Energy supply&indicator=Total primary energy supply (TPES) by source

Kushner, F., Richard, S. J., & Strickland, R. A. (2000). Critical Review of Compressor Impeller Vibration Parameters For Failure Prevention. *Proceedings of the 29th Turbomachinery Symposium*.

Oh, H. W., Yoon, E. S., & Chung, M. K. (1997). An optimum set of loss models for performance prediction of centrifugal compressors. *Proceedings of the Institution of Mechanical Engineers, Part A: Journal of Power and Energy*, *211*(4), 331–338. https://doi.org/10.1243/0957650971537231

Saravanamuttoo, H. I. H., Rogers, G. F. C., Cohen, H., Straznicky, P. V., & Nix, A. C. (2017). *Gas Turbine Theory* (7th ed.). Pearson. www.pearson.com/uk

Singh, M. P., Thakur, B. K., Sullivan, W. E., & Donanld, G. (2003). Resonance Identification For Impellers. *Proceedings of the Thirty-Second Turbomachinery Symposium*, 59–70.

Singh, M. P., Vargo, J. J., Schiffer, D. M., & Dello, J. D. (1988). Safe Diagram - A Design And Reliability Tool For Turbine Blading. *Proceedings of the 17th Turbomachinery Symposium*, 93–102. https://doi.org/10.21423/R1B673

Wang, Q., Bartos, J. C., & Houston, R. A. (1999). Methodology of Open Bladed Impeller Resonance Identification. *Proceedings of the 28th Turbomachinery Symposium*, 61–68.

White, M. T., Bianchi, G., Chai, L., Tassou, S. A., & Sayma, A. I. (2020). Review of supercritical CO2 technologies and systems for power generation. *Applied Thermal Engineering*, *185*(December 2020), 28. https://doi.org/10.1016/j.applthermaleng.2020.116447

Wright, S. A., Radel, R. F., Vernon, M. E., Pickard, P. S., & Rochau, G. E. (2010). *Operation and Analysis of a Supercritical CO2 Brayton Cycle*. https://doi.org/10.2172/984129

Yin, T., Pei, J., Yuan, S., Osman, M. K., Wang, J., & Wang, W. (2017). Fluid-structure interaction analysis of an impeller for a high-pressure booster pump for seawater desalination. *Journal of Mechanical Science and Technology*, *31*(11), 5319–5328. https://doi.org/10.1007/s12206-017-1026-z

Younsi, M., & Hypolite, E. (2019). Investigation and prediction models of the axial thrust in centrifugal compressors. *Proceedings of the ASME Turbo Expo*, *2*C-*2019*(June), 0–7. https://doi.org/10.1115/GT2019-90165

6. RESPONSIBILITY NOTICE

The authors are the only ones responsible for the printed material included in this paper.